Theor Chem Acc (2011) 130:61–68
DOI 10.1007/s00214-011-0960-6

REGULAR ARTICLE

A theoretical study on magnesium ion–selective two-photon fluorescent probe based on benzo [h] chromene derivatives

Yang Zhao · Ai-Min Ren · Lu-Yi Zou · Jing-Fu Guo · Ji-Kang Feng

Received: 29 March 2011 / Accepted: 10 May 2011 / Published online: 25 May 2011

Abstract The geometrical structure, electronic structure, and one-photon absorption (OPA) properties of a series of magnesium ion (Mg^{2+})-selective fluorescent probes based on benzo [h] chromene derivatives have been theoretically studied by using density functional theory (DFT) method and Zerner's intermediate neglect of differential overlap (ZINDO) methods. Their two-photon absorption (TPA) properties are also calculated by using the method of ZINDO/sum-over-states. Results show that all studied probe molecules exhibit large TPA cross-section (δ_{max}) in response to Mg^{2+} in 700- to 1,200-nm range. Furthermore, the δ_{max} can be greatly enhanced by introducing acceptor groups to the lateral side of benzo [h] chromene. And that probes with stronger acceptor group show larger δ_{max} and result in 70-fold enhancing when coordinate with Mg^{2+}. Significantly, probe molecules with good cell permeability were also studied by replacing the hydrogen group with acetoxymethyl ester, but δ_{max} changed slightly. These results shed light into the design strategy of efficient TP fluorescent probes with large δ_{max} and good cell permeability for Mg^{2+} sensing in living systems.

Keywords Magnesium ion · Two-photon fluorescent probe · Benzo [h] chromene derivatives · One-photon absorption · Two-photon absorption cross-section

1 Introduction

Two-photon absorption (TPA) is a nonlinear optical process first predicted theoretically by Maria Göppert-Mayer in 1931 [1]. With the development of laser technology, breakthrough progress has been made in theoretical prediction, molecular design, synthesis, and applications of TPA materials in the past decade years. Materials with large TPA cross-sections have been utilized for a myriad of optical applications such as three-dimensional (3D) optical storage memory [2, 3], upconverted lasing [4], optical power limiting [5], and photodynamic therapy [6].

Recently, because of the development of TPA materials in many different fields, more attention has been paid on its potential applications in life science. For example, optical imaging with two-photon (TP) material has become a vital tool in the investigation of living system [7–9]. Compared with one-photon microscopy, TP microscopy employing two near-infrared (NIR) photons for excitation offers many advantageous features, including the reduction of photobleaching and photodamage of imaging probes and cellular structures; high three-dimensional selectivity; the capability of penetrating thick tissues; the absorption light strength of a TPA process dependent on the square of the irradiance, which makes it possible to confine the laser excitation in a minute spatial volume [10–12]. So, TP fluorescent probes have attracted much interest and been used to clarify various biological mechanisms in living systems.

Magnesium ion (Mg^{2+}) is one of the most abundant divalent cation in living cells and plays vital roles in cell

Electronic supplementary material The online version of this article (doi:10.1007/s00214-011-0960-6) contains supplementary material, which is available to authorized users.

Y. Zhao · A.-M. Ren (✉) · L.-Y. Zou · J.-K. Feng
State Key Laboratory of Theoretical and Computational Chemistry, Institute of Theoretical Chemistry, Jilin University, Changchun 130023, Jilin, China
e-mail: aimin_ren@yahoo.com

J.-F. Guo
School of Physics, Northeast Normal University, Changchun 130021, Jilin, China

proliferation and cell death. It also involves in the maintenance of cell shape, modulation of signal transduction, various transporters, and ion channels [13–21]. The biochemistry of Mg^{2+} has been thoroughly studied in vitro, but the knowledge about its cellular homeostasis is still scarce, due to the lack of appropriate detection method. To understand its role in regulating cellular process, it is essential to monitor the Mg^{2+} concentration in the intracellular compartment as well as its distribution throughout living systems. A number of methodologies have been reported in recent years. However, many of these methodologies can be hampered by interference from Ca^{2+} for that many probes have stronger binding affinity for Ca^{2+} than for Mg^{2+}. Although some probes with β-diketone subunit can overcome this shortcoming [12, 19, 22–24], they still cannot be widely used in living systems for the insufficient sensitivity suffered from photobleaching and photodamage effects.

It is known that TP probe with large two-photon absorption cross-section (δ_{max}) is capable of imaging Mg^{2+} ions. However, their application in living tissues is still limited. In 2007, Kim et al. designed and synthesized a novel useful TP probe, which can emit strong TP-excited fluorescence in response to Mg^{2+} in the 800- to 1,000-nm range and can be easily loaded into living cell and tissue, exhibits high photostability, and can measure the Mg^{2+} concentration without interference by Ca^{2+} ions in living cells [12, 25]. However, the relationship between the probe structure and the emitting fluorescence intensity and the guidelines directed their potential applications in living systems are still unclear. Herein, we designed and theoretically studied a series of TP fluorescent probes based on benzo [h] chromene derivatives; the intrinsic relationships between molecular structure and TPA properties were revealed. It is significant that our results not only provide some useful theoretical guidelines for the design and synthesis of benzo [h] chromene derivatives with excellent TPA properties but also directed their applications in living cells.

2 Computational method

The TPA process corresponds to simultaneous absorption of two photons. The TPA efficiency of an organic molecule, at optical frequency $\omega/2\pi$, can be characterized by the TPA cross-section $\delta(\omega)$. It can be directly related to the imaginary part of the second hyperpolarizability $\gamma(-\omega; \omega, -\omega, \omega)$ [26, 27], as shown in Eq. (1):

$$\delta(\omega) = \frac{3\hbar\omega^2}{2n^2c^2\varepsilon_0} L^4 \mathrm{Im}[\gamma(-\omega;\omega,-\omega,\omega)] \quad (1)$$

where $\hbar\omega$ is the energy of the incoming photons, c is the speed of light, ε_0 is the vacuum electric permittivity, n denotes the refractive index of the medium, and L corresponds to the local-field factor. In the calculations presented here, n and L are set to 1 because the isolated molecule is in the vacuum.

The sum-over-states (SOS) expression to evaluate the components of the second hyperpolarizability $\gamma(-\omega; \omega, -\omega, \omega)$ can be educed using perturbation theory. By considering a Taylor expansion of the energy with respect to the applied field, the Cartesian components of γ are given by Refs. [28] and [29]. In the present work, all damping factors Γ are set to 0.10 eV. To compare the calculated δ value with the experimental value measured in solution, the orientationally averaged (isotropic) value of γ is evaluated, which is defined as

$$\langle\gamma\rangle = \frac{1}{15}\sum_{i,j}(\gamma_{iijj} + \gamma_{ijij} + \gamma_{ijji}) \quad i,j = x,y,z \quad (2)$$

thereafter $\langle\gamma\rangle$ is taken into expression (1) and then the TPA cross-section δ is obtained.

In the present study, the geometry optimization of all benzo [h] chromene derivatives has been carried out by using the DFT/B3LYP/6-31G* in the Gaussian 03 package of quantum chemical programs [30–32], while the UV–Vis spectrum, transition dipole moment, and the corresponding transition energy by single and double electron excitation configuration interaction have been calculated by employing the ZINDO program [33]. The CI-active spaces, for the singly excited configuration, were restricted to the 20 highest-occupied and 20 lowest-unoccupied π orbitals but were restricted to the 3 highest-occupied and 3 lowest-unoccupied π orbitals for the doubly excited configuration. Then, the values of Imγ, related to δ, were calculated by applying the FTRNLO program compiled by our group. Finally, the TPA cross-sections of all molecules are predicted.

3 Results and discussion

3.1 Molecular design

It is well known that an efficient intracellular TP probe must be endowed with large TPA cross-section, high selectivity, good water solubility, and high photostability. On this premise, we designed a series of Mg^{2+} probes on the basis of benzo [h] chromene (Fig. 1). The molecular structure of the benzo [h] chromene main body keeps a good conjugation plane to enhance its photostability [25, 34] and contains an integral β-keto acid to accept Mg^{2+} and also to increase its water solubility [23, 24]. On the other hand, it is also an efficient way to increase the potential of charge transfer efficiency and to enlarge the TPA cross-section by enhancing the substituted donor or acceptor group strength or extending the conjugation

length [35–37]. In the present study, we designed a series of Mg^{2+} probes by introducing different donor or acceptor groups or extending the conjugated length at the terminal of the cyclic planar framework aims to enhance the intramolecular charge transfer (ICT) and finally enhanced the TP response to Mg^{2+}. As shown in Fig. 1, CMg*X* denotes the designed Mg^{2+} probes, CMg*X*-Mg^{2+} are their corresponding compounds when coordinate with Mg^{2+}, and the substituted groups are also listed below for CMg*X* (*X* = 1–7). For comparison of the TPA property of molecules with different cell permeability, CMg3 was also constructed by converting the hydrogen group on R_2 position of CMg2 with acetoxymethyl ester.

3.2 One-photon absorption properties

The OPA properties of all studied molecules have been calculated by employing the ZINDO program on the basis of the equilibrium geometries calculated by DFT/B3LYP/6-31G* method. The calculated OPA wavelengths (λ^0), the corresponding oscillator strengths (*f*), and the transition natures are all listed in Table 1, and some reported experimental data are given in parentheses. The OPA wavelengths (λ^0) of CMg2, CMg2-Mg^{2+}, and CMg3 with experimental data reported were also calculated by employing TDDFT/B3LYP/6-31G* method [25]. Compared the results obtained by TDDFT and ZINDO method with the experimental results, λ^0 calculated by ZINDO method are in better agreement with the experimental values. So, it is reasonable and reliable to predict the OPA and TPA properties of the studied molecules by employing ZINDO program.

As shown in Table 1, at least two OPA peaks are existed for all the probes and these OPA peaks are mainly located near 400 nm. As the donor or acceptor group strength increased, the OPA wavelength changed slightly. However, when the styryl is introduced to the main body to extend the conjugated length, the OPA peaks of CMg4 with terminal donor group are largely red-shifted compared with CMg2. Meanwhile, more OPA peaks can be observed as the conjugated length extended. When the probes coordinate with Mg^{2+}, the OPA peaks of CMg*X*-Mg^{2+} are all red-shifted compared with their corresponding probes CMg*X*. When the lateral side group (R_1) is substituted with donor or acceptor group, the first OPA peak of CMg*X*-Mg^{2+} is mainly located around 650–700 nm and also has strong absorption band near 400 nm. Interestingly, when a styryl conjugated bridge is introduced to the probe, a strong OPA peak is observed in the NIR region for CMg*X*-Mg^{2+} complexes (CMg4-Mg^{2+}: 1,197.5 nm), although there still exist OPA peaks in lower wavelength region. In view of the results discussed above, it can be concluded that different donor or acceptor groups have less effect on the OPA properties of CMg*X*. When these probes coordinate with Mg^{2+}, a strong OPA peak will appear in the long wavelength region. But it should be noticed that when the conjugated length extended in the terminal, λ^0_{max} of CMg*X*-Mg^{2+} are largely red-shifted and located at the NIR region, which suggested that CMg4 may be potential one-photon microscopy materials.

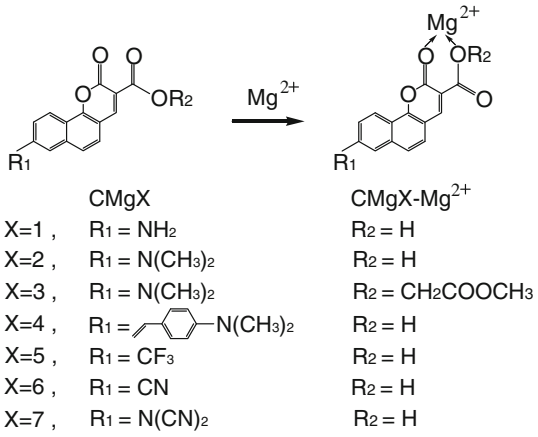

	CMgX	CMgX-Mg^{2+}
X=1 ,	$R_1 = NH_2$	R_2 = H
X=2 ,	$R_1 = N(CH_3)_2$	R_2 = H
X=3 ,	$R_1 = N(CH_3)_2$	$R_2 = CH_2COOCH_3$
X=4 ,	R_1 =	R_2 = H
X=5 ,	$R_1 = CF_3$	R_2 = H
X=6 ,	R_1 = CN	R_2 = H
X=7 ,	$R_1 = N(CN)_2$	R_2 = H

Fig. 1 Molecular structures of studied Mg^{2+} probes (CMg*X*) and their corresponding Mg^{2+} binding compounds (CMg*X*-Mg^{2+})

3.3 Two-photon absorption properties

On the basis of correct OPA spectrum, the TPA properties of CMg*X* and CMg*X*-Mg^{2+} are calculated by using ZINDO-SOS method. In consideration of its applicability in the living systems of the TP probes with lower excitation energy, the TPA properties in the range of 700–1,200 nm of studied molecules were discussed in this work. Table 2 summarizes the calculated results of TPA wavelengths (λ^T_{max}) and δ_{max}. It can be seen that as the donor group strength increased, the δ_{max} of CMg2 increased slightly compared with CMg1. Their corresponding Mg^{2+} binding complex CMg2-Mg^{2+} and CMg1-Mg^{2+} show the same trend, but about 7 times enhancement in δ_{max} compared with their corresponding probe-unbound Mg^{2+}. It means that the δ_{max} increased greatly in response to Mg^{2+}. Similarly, the δ_{max} of CMg*X*-Mg^{2+} can be further increased by increasing the acceptor group strength. However, there are little changes in δ_{max} for CMg*X* when R_1 is substituted by strong acceptor groups. From CMg5 to CMg7, the increasing in δ_{max} in response to Mg^{2+} is varied from 40- to 70-fold. So, the δ_{max} of probes CMg*X* show a dramatically enhancement in response to Mg^{2+} with the acceptor group strength increased. When R1 is substituted by donor groups, the enhancement of δ_{max} is just sevenfold and basically no change occurred as the donor group strength increased. It demonstrates that probes with terminal acceptor groups are more sensitive to Mg^{2+}. Compared

Table 1 OPA properties of studied Mg^{2+} probes

CMg*X*	Transition	λ^0_{max}/nm	*f*	CMg*X*-Mg^{2+}	Transition	λ^0_{max}/nm	*f*
CMg1	$S_0 \rightarrow S_2$	409.6	0.25585	CMg1-Mg^{2+}	$S_0 \rightarrow S_1$	687.4	0.33219
	$S_0 \rightarrow S_7$	320	0.42673		$S_0 \rightarrow S_6$	445.8	0.20122
					$S_0 \rightarrow S_{11}$	361.4	0.19258
CMg2	$S_0 \rightarrow S_2$	403.1	0.28698	CMg2-Mg^{2+}	$S_0 \rightarrow S_2$	708.8	0.32995
		(413^{exp}, [25] 382.5^{TDDFT})			$S_0 \rightarrow S_6$	454.7	0.18352
	$S_0 \rightarrow S_7$	314.5	0.37689			(443^{exp}, [25] 482.6^{TDDFT})	
					$S_0 \rightarrow S_9$	372.9	0.14385
CMg3	$S_0 \rightarrow S_2$	425.7	0.27779	CMg3-Mg^{2+}	$S_0 \rightarrow S_1$	690.2	0.38973
		(460^{exp}, [25] 407.9^{TDDFT})			$S_0 \rightarrow S_4$	441.8	0.16405
	$S_0 \rightarrow S_7$	324	0.39169		$S_0 \rightarrow S_7$	375.6	0.15639
					$S_0 \rightarrow S_{11}$	325	0.26425
CMg4	$S_0 \rightarrow S_1$	464.2	0.28944	CMg4-Mg^{2+}	$S_0 \rightarrow S_2$	1,197.5	0.88431
	$S_0 \rightarrow S_2$	445.3	0.5319		$S_0 \rightarrow S_4$	780.5	0.124
	$S_0 \rightarrow S_4$	367.8	0.33861		$S_0 \rightarrow S_8$	536.4	0.13088
	$S_0 \rightarrow S_5$	355.5	0.20382		$S_0 \rightarrow S_{10}$	506.3	0.12041
	$S_0 \rightarrow S_9$	329.8	0.38186		$S_0 \rightarrow S_{18}$	375	0.17084
CMg5	$S_0 \rightarrow S_2$	371.3	0.23058	CMg5-Mg^{2+}	$S_0 \rightarrow S_1$	647.9	0.18879
	$S_0 \rightarrow S_7$	309.2	0.51409		$S_0 \rightarrow S_6$	445.2	0.19678
					$S_0 \rightarrow S_{10}$	368.2	0.3552
CMg6	$S_0 \rightarrow S_2$	368.5	0.30925	CMg6-Mg^{2+}	$S_0 \rightarrow S_1$	659.3	0.11944
	$S_0 \rightarrow S_8$	308	0.58955		$S_0 \rightarrow S_2$	594.6	0.25058
					$S_0 \rightarrow S_5$	476	0.2338
					$S_0 \rightarrow S_{10}$	373.6	0.38546
CMg7	$S_0 \rightarrow S_2$	372.4	0.26676	CMg7-Mg^{2+}	$S_0 \rightarrow S_1$	655	0.18906
	$S_0 \rightarrow S_9$	310.1	0.54009		$S_0 \rightarrow S_2$	605.7	0.16774
					$S_0 \rightarrow S_6$	447	0.18596
					$S_0 \rightarrow S_{12}$	373.1	0.22231

with CMg2, CMg4 with an extended conjugation length shows a red-shifted λ^T_{max} and a greatly enhanced δ_{max} in response to Mg^{2+}. The increasing in δ_{max} of CMg4-Mg^{2+} is about 20-fold. So, it is more sensitive to Mg^{2+} when the probe conjugation length is extended.

In order to explain the origin of TPA properties of the investigated molecules, a two-level model was adopted, in which the TPA cross-section can be defined as [36, 38–40]

$$\delta = \frac{4\pi^2 a_0^5 \alpha \omega^2}{15 c_0} \frac{M_{0n}^2 \Delta\mu_{0n}^2}{E_{0n}^2 \Gamma} \tag{3}$$

where a_0 is the Bohr radius, c_0 is the speed of the light, α is the fine structure constant, ω is the photon energy, M_{0n} is the transition dipoles between the ground state $|0>$ and $|a>$ TPA final state $|n>$, $\Delta\mu_{0n}$ is the dipole moment difference between ground and excited states, and E_{0n} is the transition energy between the ground states $|0>$ and a TPA final state $|n>$. The formula (3) can be simplified to the following formula

$$\delta \propto \frac{M_{0n}^2 \Delta\mu_{0n}^2}{E_{0n}^2 \Gamma} \tag{4}$$

As discussed above, that probe with different lateral side groups exerted little differences on δ_{max}. But for their corresponding Mg^{2+} binding complexes, this difference is more obvious. In order to analyze the relationship between δ values and molecular structures using the two-level model, all related parameters of CMg*X*-Mg^{2+} are listed in Table 3. Insight into these parameters, we can found that as the strength of donor group increased and the conjugated length extended, M_{0n} and $\Delta\mu_{0n}$ show an apparent enhancement, while E_{0n} decreased gradually.

The same tendency can be observed for M_{0n}, $\Delta\mu_{0n}$, and E_{0n} when the acceptor group strength increased at the molecular terminal, except for the $\Delta\mu_{0n}$ of CMg5-Mg^{2+} and M_{0n} of CMg7-Mg^{2+}. According to Eq. 4, δ is in proportion to the product of M_{0n} and $\Delta\mu_{0n}$, while it is in inverse proportion to E_{0n}. The relationship between the

Table 2 TPA properties of studied Mg^{2+} probes in the NIR region

CMg*X*	λ_{max}^{T}/nm	δ/GM	CMg*X*-Mg^{2+}	λ_{max}^{T}/nm	Imγ	δ/GM	Channel
CMg1	817.84	30.76	CMg1-Mg^{2+}	817.84	8,995	221.81	$S_0 \rightarrow S_7$ H-2 → L+1 24% H → L+3 24% H → L+6 10% H, H → L+1, L+1 19%
CMg2	805.1 820[exp] [25]	37.85 84[exp] [25]	CMg2-Mg^{2+}	844.58 880[exp] [25]	10,645	246.15 107[exp] [25]	$S_0 \rightarrow S_7$ H-2 → L+1 21% H → L+3 22% H → L+6 12% H, H → L+1, L+1 18%
CMg3	851.55	43.2	CMg3-Mg^{2+}	827.67	14,519	349.58	$S_0 \rightarrow S_5$ H-2 → L+1 15% H → L+3 31% H → L+5 11% H, H → L+1, L+1 12%
CMg4	891.98	171.15	CMg4-Mg^{2+}	884.34	163,494	3,448.25	$S_0 \rightarrow S_{12}$ H → L+4 13% H → L+6 18%
CMg5	741.54	18.44	CMg5-Mg^{2+}	738.89	22,560	681.6	$S_0 \rightarrow S_9$ H → L+3 32% H → L+5 41%
CMg6	736.25	18.74	CMg6-Mg^{2+}	746.9	28,454	841.33	$S_0 \rightarrow S_{10}$ H-3 → L+1 37% H → L+5 18%
CMg7	744.21	21.21	CMg7-Mg^{2+}	749.61	54,119	1,588.62	$S_0 \rightarrow S_{12}$ H-7 → L+1 16% H-2 → L+1 27% H → L+5 15%

H, H-*n*, L, and L+*n* denote HOMO, HOMO-*n*, LUMO, and LUMO+*n*, respectively

Table 3 The related parameters for CMg*X*-Mg^{2+} using the two-level model

Compound	M_{0n}	$\Delta\mu_{0n}$	E_{0n}	δ
CMg1-Mg^{2+}	1.04	4.47	3.04	221.81
CMg2-Mg^{2+}	1.49	5.30	2.94	246.15
CMg3-Mg^{2+}	1.16	5.38	3.00	349.58
CMg4-Mg^{2+}	3.81	10.06	2.76	3,448.25
CMg5-Mg^{2+}	1.95	6.79	3.33	681.60
CMg6-Mg^{2+}	5.53	4.21	3.32	841.33
CMg7-Mg^{2+}	4.20	5.12	3.32	1,588.62

δ_{max} of CMg*X*-Mg^{2+} and $M_{0n}^2\Delta\mu_{0n}^2/E_{0n}^2\Gamma$ is depicted in Fig. 2. We can found that the calculated points are averagely distributed on the two sides of the fitted line, which further confirmed the above conclusions. So, the results analyzed above indicated that the changes in δ_{max} can be predicted by the two-level model, and M_{0n}, $\Delta\mu_{0n}$, and E_{0n} are all important factors to δ_{max} of the Mg^{2+} binding complexes.

ICT is another important factor that affects the change in TPA cross-section. In order to further interpret the internal factors that affect the TPA properties, the frontier orbitals' contour surfaces of the probes and their corresponding

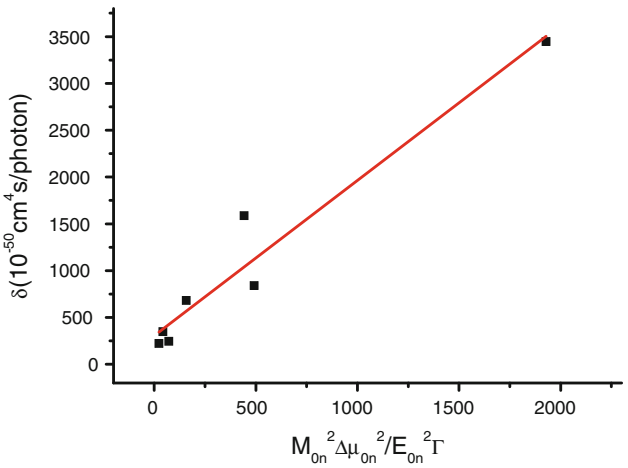

Fig. 2 Plot of δ_{max} versus $M_{0n}^2\Delta\mu_{0n}^2/E_{0n}^2\Gamma$

Mg^{2+} complexes related to the TPA process were also investigated. The molecular orbitals related to the main transitions of TPA process are shown in Fig. 3.

The main configuration of all probes before they coordinate with Mg^{2+} is HOMO → LUMO. It can be found that almost all electron densities of these probes' HOMO and LUMO are distributed averagely on the whole molecule and no obvious electron transfer occurred during the TPA process, so their δ values are not too large and the

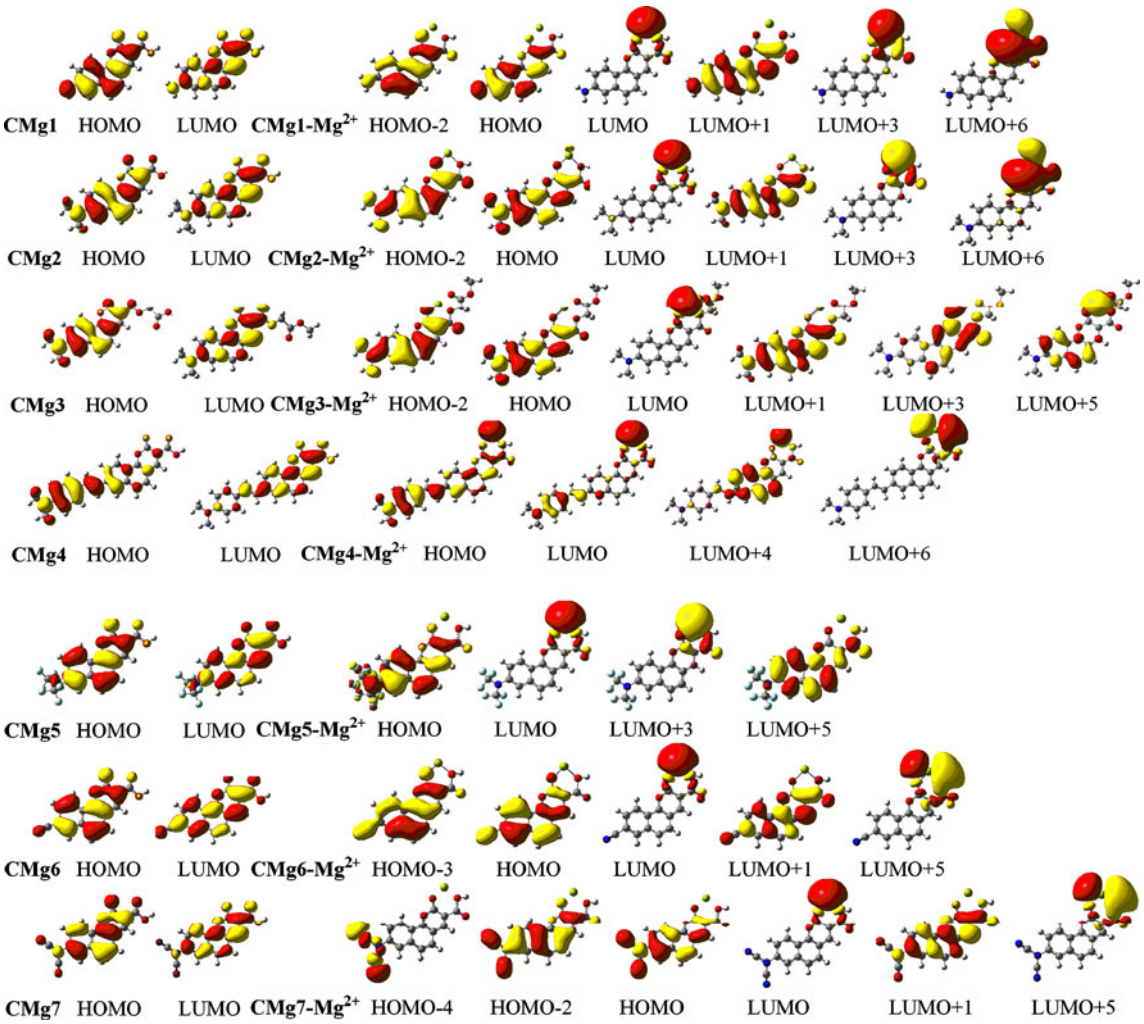

Fig. 3 Contour surfaces of the frontier orbital relevant to the maximum TPA for the studied molecules

differences among them are unobvious except for molecule CMg4 that δ is apparently larger than other probes. This is attributed to the apparent charge transfer between the lateral side donor group and the main body benzo [h] chromene during the TPA process as illustrated in Fig. 3. When these probes coordinate with Mg^{2+}, apparent electron transfer must be occurred between the benzo [h] chromene main body and Mg^{2+} during the TPA process, which will be resulted in large TPA cross-sections. From Fig. 3, we can also found that the electron density of the occupied orbitals of Mg^{2+} complexes increased obviously when introducing strong electron donor or acceptor groups or extending the molecular conjugated length. But the electron density is mainly concentrated on the molecular main body, while hardly distributed on Mg^{2+}. For the complexes with terminal acceptor groups, the electron densities more prefer to distribute near the acceptor groups, and the centralized tendency becomes more obvious as the acceptor group strength increases. However, the electron densities of all of the Mg^{2+} complexes' unoccupied orbital are mainly concentrated on Mg^{2+}. Almost no electron densities distribute on the molecular framework, even though the terminal acceptor groups are introduced. We can deduce that Mg^{2+} plays an important role as a strong acceptor group in these complexes and its electron-withdrawing ability is stronger enough to attract electrons from the terminal groups. This leads that the M_{0n} of the complexes with terminal acceptor groups are larger than those with donor groups. Finally, the variation in electron density and M_{0n} resulted in different TPA responses to Mg^{2+}. According to the results discussed above, we can conclude that (1) increasing the acceptor group strength or introducing the conjugated segment can cause the Mg^{2+} complexes to show high electron transfer efficiency and result in a dramatically enlarged δ_{max}; (2) the electron transfer efficiency are more obvious during the TPA process for the complexes with terminal acceptor groups, so they are more sensitive to Mg^{2+}; (3) for CMg3-Mg^{2+}, there is almost no

electron density distributed on the occupied and unoccupied orbitals of the acetoxymethyl ester, and there are little changes occurred in the electron density distribution by replacing the hydrogen group with acetoxymethyl ester. So, the δ_{max} of CMg2-Mg^{2+} and CMg3-Mg^{2+} did not change significantly.

4 Conclusion

In summary, we theoretically studied the geometrical structure, OPA and TPA properties, and electronic structure of a series of magnesium ion–selective fluorescent probe based on benzo [h] chromene derivatives. Calculated results showed that almost all probes exhibit large TPA cross-sections in response to Mg^{2+} in 700- to 1,200-nm range. However, introducing donor groups to benzo [h] chromene main body cannot greatly enhance the δ_{max} of the probes, sevenfold enhancement was observed only when they coordinate with Mg^{2+}, and not too much change occurred by increasing the donor group strength. When acceptor group was introduced to the benzo [h] chromene main body, the increasing in δ_{max} for Mg^{2+} binding complexes varied from about 40- to 70-fold as the acceptor group strength increased. These results suggest that the benzo [h] chromene-based derivatives with terminal acceptor groups are more efficient TP fluorescence probes for Mg^{2+}. Furthermore, probes with different cell permeability were also studied by replacing the hydrogen group with acetoxymethyl ester, and results showed that little change occurred on δ_{max} for both the probe and its corresponding Mg^{2+} binding complexes. Through the analysis of the frontier orbitals' contour surfaces, we can also find that different responses to Mg^{2+} are mainly caused by the variation in electron density and M_{0n} during the TPA process. This work not only provides useful theoretical guidelines to the design of benzo [h] chromene derivatives with excellent TPA properties but also sheds light into the significance of the benzo [h] chromene derivatives as promising Mg^{2+} fluorescent probes in living systems.

Acknowledgments This work was supported by the National Nature Science Foundation of China (20673045, 20973078) and the Open Project of the State Key Laboratory of Superamolecular Structure and Materials of Jilin University (SKLSSM200716).

References

1. Göppert-Mayer M (1931) Ann Phys 401:273–294
2. Dvornikov AS, Rentzepis PM (1995) Opt Commun 119:341–346
3. Cumpston BH, Ananthavel SP, Barlow S, Dyer DL, Ehrlich JE, Erskine LL, Heikal AA, Kuebler SM, Lee IYS, Maughon MD, Qin J, Rockel H, Rumi M, Wu X-L, Marder SR, Perry JW (1999) Nature 398:51–54
4. Fleitz PA, Brant MC, Sutherland RL, Strohkendl FP, Larson RJ, Dalton LR (1998) SPIE Proc 3472:91–97
5. Ehrlich JE, Wu XL, Lee LY, Hu ZY, Rockel H, Marder SR, Perry JW (1997) Opt lett 22:1843–1845
6. Denk W, Strickler JH, Webb WW (1990) Science 248:73–76
7. Kim HM, Cho BR (2009) Acc Chem Res 42:863–872
8. Sumalekshmy S, Fahrni CJ (2011) Chem Mater 23:483–500
9. Kim HM, Cho BR (2011) Chem Asian J 6:58–69
10. Zipfel WR, Williams RM, Webb WW (2003) Nat Biotechnol 21:1369–1377
11. Helmchen F, Denk W (2005) Nat Methods 2:932–940
12. Kim HM, Jung C, Kim BR, Jung S-Y, Hong JH, Ko Y-G, Lee KJ, Cho BR (2007) Angew Chem Int Ed 46:3460–3463
13. Hartwig A (2001) Mutat Res 475:113–121
14. O'Rourke B, Backx PH, Marban E (1992) Science 257:245–248
15. Politi HC, Preston RR (2003) Neuroreport 14:659–668
16. Dai L-J, Ritchie G, Kerstan D, Kang HS, Cole DEC, Quamme GA (2001) Physiol Rev 81:51–84
17. Schmitz C, Perraud A, Johnson CO, Inabe K, Smith MK, Penner R, Kurosaki T, Fleig A, Scharenberg AM (2003) Cell 114:191–200
18. Wolf FI, Torsello A, Fasanella S, Cittadini A (2003) Mol Aspects Med 24:11–26
19. Ray D, Bharadwaj PK (2008) Inorg Chem 47:2252–2254
20. Romani A, Scarpa A (1992) Arch Biochem Biophys 298:1–12
21. Shoda T, Kikuchi K, Kojima H, Urano Y, Komatsu H, Suzukic K, Nagano T (2003) Analyst 128:719–723
22. Farruggia G, Iotti S, Prodi L, Montalti M, Zaccheroni N, Savage PB, Trapani V, Sale P, Wolf FI (2006) J Am Chem Soc 128:344–350
23. Suzuki Y, Komatsu H, Ikeda T, Saito N, Araki S, Citterio D, Hisamoto H, Kitamura Y, Kubota T, Nakagawa J, Oka K, Suzuki K (2002) Anal Chem 74:1423–1428
24. Komatsu H, Iwasawa N, Citterio D, Suzuki Y, Kubota T, Tokuno K, Kitamura Y, Oka K, Suzuki K (2004) J Am Chem Soc 126:16353–16360
25. Kim HM, Yang PR, Seo MS, Yi J-S, Hong JH, Jeon S-J, Ko Y-G, Lee KJ, Cho BR (2007) J Org Chem 72:2088–2096
26. Cha M, Torruellas WE, Stegeman GI, Horsthuis WHG, Möhlmann GR, Meth J (1994) Appl Phys Lett 65:2648–2650
27. Kogej T, Beljonne D, Meyers F, Perry JW, Marderm SR, Brédas JL (1998) Chem Phys Lett 298:1–3
28. Orr BJ, Ward JF (1971) Mol Phys 20:513–526
29. Bishop DM, Luis JM, Kirtman B (2002) J Chem Phys 116:9729–9739
30. Becke AD (1993) J Chem Phys 98:1372–1377
31. Francl MM, Pietro WJ, Hehre WJ, Binkley JS, Gordon MS, Defrees DJ, Pople JA (1982) J Chem Phys 77:3654–3665
32. Frisch MJ, Trucks GW, Schlegel HB, Scuseria GE, Robb MA, Cheeseman JR, Montgomery JA, Vreven TJ, Kudin KN, Burant JC, Millam JM, yengar SS, Tomasi J, Barone V, Mennucci B, Cossi M, Scalmani G, Rega N, Petersson GA, Nakatsuji H, Hada M, Ehara M, Toyota K, Fukuda R, Hasegawa J, Ishida M, Nakajima T, Honda Y, Kitao O, Nakai H, Klene M, Li X, Knox JE, Hratchian HP, Cross JB, Adamo C, Jaramillo J, Gomperts R, Startmann RE, Yazyev O, Austin AJ, Cammi R, Pomelli C, Ochterski JW, Ayala PY, Morokuma K, Voth GA, Salvador P, Dannenberg JJ, Zakrzewski VG, Dapprich JM, Daniels AD, Strain MC, Farkas O, Malick DK, Rabuck AD, Raghavachari K, Foresman JB, Ortiz JV, Cui Q, Baboul AG, Cliffors S, Cioslowski J, Stefanov BB, Liu G, Liashenko A, Piskorz I, Komaromi I, MartinR L, Fox DJ, Keith T, Al-Laham MA, Peng CY, Manayakkara A, Challacombe M, Gill PMW, Johnson BG, Chen

W, Wong MW, Gonzalez C, PopleJA (2003) Gaussian revision C. 02; Gaussian, Inc., Pittsburgh
33. Ridley J, Zerner MC (1973) Theo Chim Acta 32:111–134
34. Kim HM, Yang WJ, Kim CH, Park W-H, Jeon S-J, Cho BR (2005) Chem Eur J 11:6386–6391
35. Albota M, Beljonne D, Brédas JL, Ehrlich JE, Fu JY, Heikal AA, Hess SE, Kogej T, Levin MD, Marder SR, McCord-Maughon D, Perry JW, Rockel H, Rumi M, Subramaniam G, Webb WW, Wu XL, Xu C (1998) Science 281:1653–1656
36. Òscar RP, Luo Y, Ågren H (2006) J Chem Phys 124:094310-1–094310-5
37. Ma WB, Wu YQ, Gu DH, Gan FX (2006) J Mol Struct (Theochem) 772:81–87
38. Guo J-D, Wang C-K, Luo Y, Ågren H (2003) Phys Chem Chem Phys 5:3869–3873
39. Luo Y, Oscar RP, Guo JD, Ågren H (2005) J Chem Phys 122:096101-1–096101-2
40. Li WC, Feng JK, Ren AM, Zhang XB, Sun CC (2009) Chinese Physics B 18:2271–2281